

# Adaptive Beamforming of a Towed Array During a Turn

Peter Gerstoft, William S. Hodgkiss, *Member, IEEE*, W. A. Kuperman, Heechun Song, *Member, IEEE*,  
Martin Siderius, and Peter Loring Nielsen

**Abstract**—During maneuvering, towed array beamforming degrades if a straight array is assumed. This is especially true for high-resolution adaptive beamforming. It is experimentally demonstrated that adaptive beamforming is feasible on a turning array, provided that array shape is estimated. The array shape can be inferred solely from the coordinates of the tow vessel's Global Positioning System (GPS) without any instrumentation in the array. Based on estimated array shape from the GPS, both the conventional beamformer and the white noise constrained (WNC) adaptive beamformer are shown to track the source well during a turn. When calculating the weight vector in the WNC approach, a matrix inversion of the cross-spectral density matrix is involved. This matrix inversion can be stabilized by averaging the cross-spectral density matrix over neighboring frequencies. The proposed algorithms have been tested on real data with the tow-vessel making 45° turns with a 500-m curvature radius. While turning, the improvement in performance over the assumption of a straight array geometry was up to 5 dB for the conventional beamformer and considerably larger for the WNC adaptive beamformer.

**Index Terms**—Adaptive beamforming, array shape estimation, curved array, global positioning system (GPS), towed array, white noise constrained (WNC).

## I. INTRODUCTION

CURRENT trends in passive sonar systems include the use of large aperture arrays with many elements to form narrow beams in order to detect quiet fast moving targets in a noisy background [1], [2]. Such a scenario often leads to “snapshot deficient” processing, meaning that the available observation time is not sufficiently large to build a well-estimated covariance matrix that can be used for standard adaptive array-processing methods. A long, turning array is a good example of a snapshot deficient case.

During maneuvering, a horizontal line array will not be straight and this will cause performance degradation for beamforming acoustic signals [3], [4]. This degradation will be more severe for adaptive beamformers which are more sensitive to errors in hydrophone location. Thus, it is important to determine the array shape during maneuvering. There has been

a significant effort to determine the array shape by acoustic means [5]–[11]. Other efforts are to model the dynamics of the array [12], [13] and to equip the array with sensors, e.g., [14]–[16].

However, few experimental data are reported in the open literature using a horizontal line array during a turn. Felisberto and Jesus [15] examined a turning array using conventional beamforming while focusing on their sensor instrumentation in the array. They used these sensors to estimate the array shape, and the left/right ambiguity was resolved during a turn.

Ferguson [6], [7] performed adaptive beamforming on a turning array whose shape was estimated either by Bucker's sharpness method [5] or based on the first eigenvector of the cross-spectral density matrix. To experimentally verify adaptive beamforming during a turn SACLANTCEN and Marine Physical Laboratory, as part of a larger geoacoustic inversion experiment, collected horizontal array data during a turn.

Based on simplifications of the Paidoussis equations and verified experimentally, Kennedy [17] showed that the shape of the array corresponds to the track of the ship under some conditions. This is the so-called “water pulley” model that is “the tow vessel bores a hole in the water and the cable simply follows though that hole” [17]. The conditions for the validity of the water pulley model is described by Kennedy [17] and Dowling [18]. For the present experiment, the water pulley model was proven to work well, as will be shown in Section V.

Knowing the coordinates of the ship from the global positioning system (GPS), it is straightforward to estimate array shape based on the water pulley model. The array shape is fitted to a parabolic shape and this approach is preferable for three reasons.

- 1) The parabola is able to describe the salient features of the bowed array. If more accuracy is needed, higher order polynomials could be used.
- 2) The parabola serves as a regularization operator of the noisy and sparsely sampled GPS measurements.
- 3) The parabola is analytically tractable.

The gain of having this accurately estimated array shape during turns will then be demonstrated using both the conventional beamformer and the white noise constrained (WNC) adaptive beamformer [19], [20]. When calculating the weight vector in the WNC approach, a matrix inversion of the cross-spectral density matrix (CSDM) is involved. This matrix inversion can be unstable due to the snapshot deficiency. The snapshot deficiency of the CSDM is mitigated here by frequency averaging over the neighboring CSDM [21], [22].

Manuscript received June 25, 2002; revised October 24, 2002. This work was supported by the Office of Naval Research under Code 32.

P. Gerstoft, W. S. Hodgkiss, W. A. Kuperman, and H. Song are with Marine Physical Laboratory, University of California at San Diego, La Jolla, CA 92093-0238 USA (e-mail: gerstoft@mpl.ucsd.edu).

M. Siderius was with SACLANT Undersea Research Centre, 19138 La Spezia, Italy. He is now with Science Applications International Corporation (SAIC), San Diego, CA 19121 USA.

P. L. Nielsen is with SACLANT Undersea Research Centre, 19138 La Spezia, Italy.

Digital Object Identifier 10.1109/JOE.2002.808203

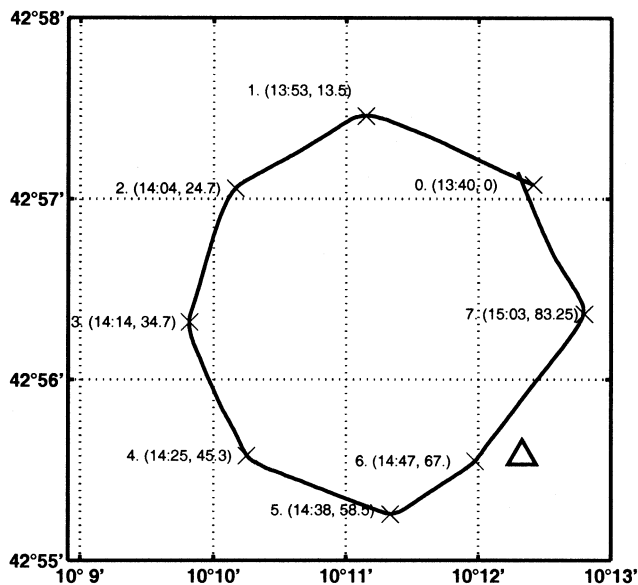


Fig. 1. Detailed map of the octagon track. The ALLIANCE sailed counterclockwise, starting in the NE corner at 13:32. The seven turns (time, time-delay in min) in the octagon also are shown. Each turn should be about  $45^\circ$ , but there is variation between the turns; turn 6 is only about  $20^\circ$  and turn 7 about  $80^\circ$ . Source ship MANNING (triangle) is moored.

## II. EXPERIMENT

The experiment was carried out off the west coast of Italy in order to investigate towed array beamforming methods especially while the array is turning. On November 28, 2000, the research vessel MANNING (triangle in Fig. 1) was moored in the North Elba area in 117-m-deep water. MANNING had lowered a source to a 50-m depth transmitting a 1-s 150–500-Hz LFM sequence every 15 s. At that time, the ALLIANCE was following a complex track involving both straight lines and maneuvering. This paper is focused on the octagon track shown in Fig. 1, where the ALLIANCE made seven  $45^\circ$  turns with a 500-m curvature radius. The octagon track covers 96 min of data, corresponding to 375 pings. The ALLIANCE was towing a 254-m-long horizontal line array (HLA) at a 55-m depth and 350 m behind the center of the ship (GPS antenna). One hundred twenty-eight hydrophones were spaced equidistantly along the array. The speed of ALLIANCE was nearly constant at 4 kn (2 m/s). A 4-s time interval around each pulse (1 s plus multipath) was sampled at 6000 Hz. Typically, the single-element SNR ratio was 30 dB at 375 Hz.

The geoacoustic bottom is similar to the one in [23]. The ocean sound-speed profile was nearly constant at 1520 m/s for the first 100 m, and thereafter the sound speed had a rapid decrease to 1510 m/s. The sediment layer was very thin (about 2 m) and the bottom was quite hard (1600 m/s). The bottom was very flat and no out-of-plane scattering was expected. At the ranges considered, it was not easy to identify individual arrivals.

## III. ARRAY MODEL

A simple model for the horizontal line array is a “water-pulley” model, where the track of the cable follows the track of the ship [17]. Thus, changes in the ships heading travel down the cable with the same speed (2 m/s) as

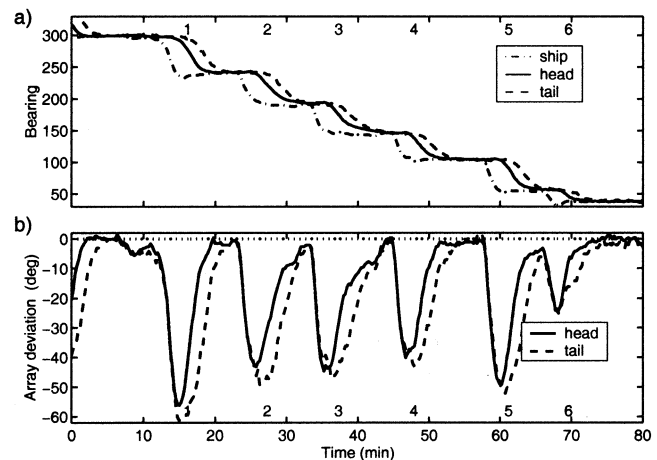


Fig. 2. Compass bearing for ship and horizontal array. (a) Ship (dash-dotted), head array (solid), and tail array (dashed). (b) Deviation between ship and head array bearing (solid), and ship and tail array bearing (dashed). Note that the seven turns are indicated at the corresponding time delay from beginning of the octagon track.

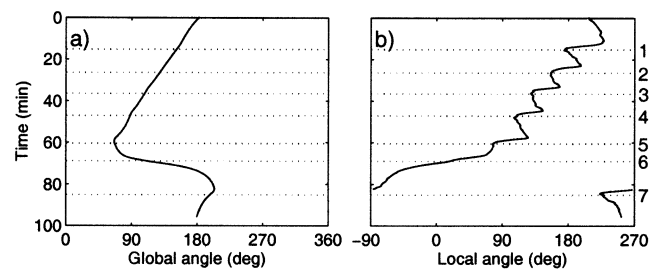


Fig. 3. Angle to MANNING (a) in a global coordinate system with North being  $0^\circ$  and (b) relative to the bearing of the ship.

the tow ship. This model seems sufficient as the dimensionless cable frequency is sufficiently low [17], [18] and by the regularity in the change in compass heading [see Fig. 2(a)]. First, the ALLIANCE (dash-dotted line) changes course, then  $(350 \text{ m})/(2 \text{ m/s}) = 4 \text{ min}$  later the front of the array (solid) changes its heading and, finally,  $(254 \text{ m})/(2 \text{ m/s}) = 2.1 \text{ min}$  later the tail of the array (dashed) changes heading. This simple transition is also clear in Fig. 2(b) where deviations from the ships heading for the head (solid) and tail (dashed) compasses are plotted. It takes ALLIANCE about 2 min to do a  $45^\circ$  turn in the octagon. From this discussion, it is clear that the array is curved or misaligned relative to the ship for about 8 min following the start of a turn, in agreement with Fig. 2.

Knowing the GPS position of ALLIANCE and MANNING, it is relatively easy to estimate the bearing to MANNING either in a global coordinate system defined relative to North (true bearing) [Fig. 3(a)] or in the local coordinate system defined by the heading of the ship [Fig. 3(b)].

The geometry is shown in Fig. 4. The main coordinate system has the  $x_V$  axis pointing in the aft direction from the vessel. The mathematical model is developed in detail in the Appendix.

The turning array is modeled as a rotation  $\beta$  around the first hydrophone from the ship's aft heading to the axis defined by the first and last hydrophone and a parabolic bow  $a$  [see Fig. 4(a)]. Whereas Bucker and Baxley [24] used a polynomial series and numerical integration to describe the array shape, here a more

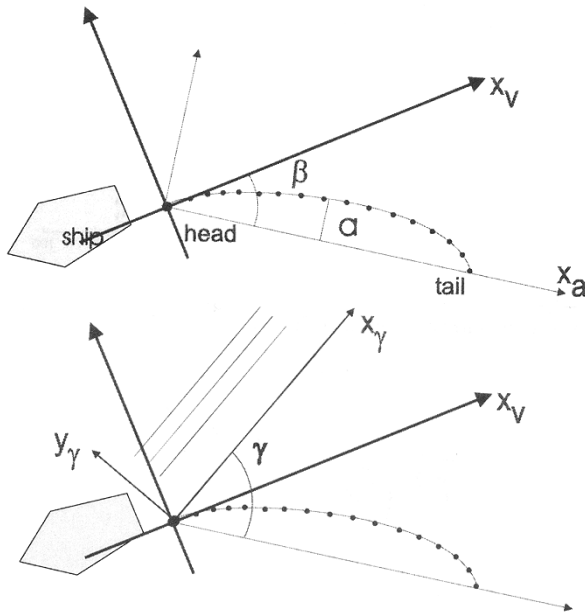


Fig. 4. Definition of coordinate systems. (a) Coordinate system for array shape. (b) Coordinate system for beamforming. In this coordinate system,  $\gamma$  corresponds to the angle of the wavefront with respect to the  $x_a$  axis. Thus,  $\gamma = \{-90^\circ, 270^\circ\}$  corresponds to tail endfire of the array,  $\gamma = 0^\circ$  broadside right,  $\gamma = 180^\circ$  broadside left, and  $\gamma = 90^\circ$  head endfire.

simple and analytically tractable parabolic shape is used [25]. In a local coordinate system with the  $x_a$  axis passing through first and last hydrophone of the array [Fig. 4(a)], the offsets ( $y$  coordinate) of each array element are given by

$$y_a = \frac{4a}{L_a^2} (L_a - x_a)x_a \quad (1)$$

where  $L_a$  is the projection of the array along the  $x_a$  axis. To second order in  $a$ , the arc length of the array  $L_s$  (this also is the length of the straight array) is related to  $L_a$  as

$$L_s \approx L_a + \frac{8}{3} \frac{a^2}{L_a}. \quad (2)$$

Using this formula, the  $x$  coordinate of each element for a bowed array  $x_a$  can be related to the element position along a straight array  $x_s$  as

$$x_a = x_s \frac{L_a}{L_s}. \quad (3)$$

For small curvatures, the correction for the  $x$ -axis element position due to the  $y$  offset is not important and is often neglected. However, when the array is turning this correction can be important, as the array deformation exceeds several wavelengths at the array design frequency. In the examples presented here, it represents a correction of five wavelengths at the array design frequency.

A plane wave impinging at an angle  $\gamma$  between the wavefront and the array ( $x_a$  axis) will see an equivalent array where the  $x_\gamma$  axis is parallel to the wavefront and the  $y_\gamma$  axis is perpendicular [Fig. 4(b)]. Only the direction perpendicular to the wavefront  $y_\gamma$  gives a phase difference across the array. Using  $x_s = nd$ , where

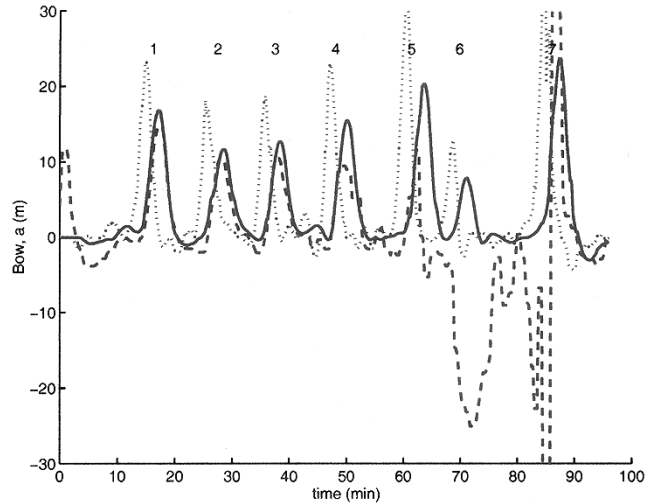


Fig. 5. Estimated equivalent bow of array with acoustics (dashed line) and GPS (solid line). For reference, the initial GPS estimate (dotted line) is also shown.

$n = \{0, \dots, 127\}$  and  $d$  is the element spacing,  $y_\gamma$  is (see the Appendix)

$$y_\gamma = -\frac{4a \cos \gamma}{L_s^2} (dx_i)^2 + dx_i \left[ \frac{4a \cos \gamma}{L_s^2} + \sin \gamma \right]. \quad (4)$$

It is observed that, while the array has a geometric bow  $a$ , the “acoustic bow” as seen from a plane wave impinging on the array is  $a \cos \gamma$ . This bow depends on the angle to the array and, as expected, the largest acoustic bow is found when the plane wave is impinging broadside ( $\gamma = 0$ ) on the array.

Finally, it should be noted that the array is rotated an angle  $\beta$  relative to the center of the ship.

#### IV. ESTIMATING ARRAY SHAPE FROM THE GPS

##### A. Array Angle $\beta$

Often there are compasses in the array and the difference between these and the course of the ship can determine the angle  $\beta$  (see Fig. 2). Alternatively, it can be determined by time delaying the ship's GPS coordinates, just as done for the array bow.  $\beta$  is not important for the processing.

##### B. Array Bow $a$

The shape of the array can be modeled using the “water-pulley model” [17] where the array follows the same trajectory as the ship. The sampling frequency of the GPS was every 15 s, corresponding to each acoustic transmission. The array shape is modeled semi-empirically by:

- 1) Time delaying the ship's GPS coordinates to the start of the horizontal array. The start of the array is 350 m behind the ship, thus the time delay is  $350/v(t)$ , where  $v(t)$  is the ship speed. For the ship speed used (about 4 kn), this corresponds to about 11 GPS points.
- 2) Estimating the parabola based on a least squares fit to the GPS points along the array (254 m). This corresponds to about seven GPS points. Both bow  $a$  and angle  $\beta$  are determined.

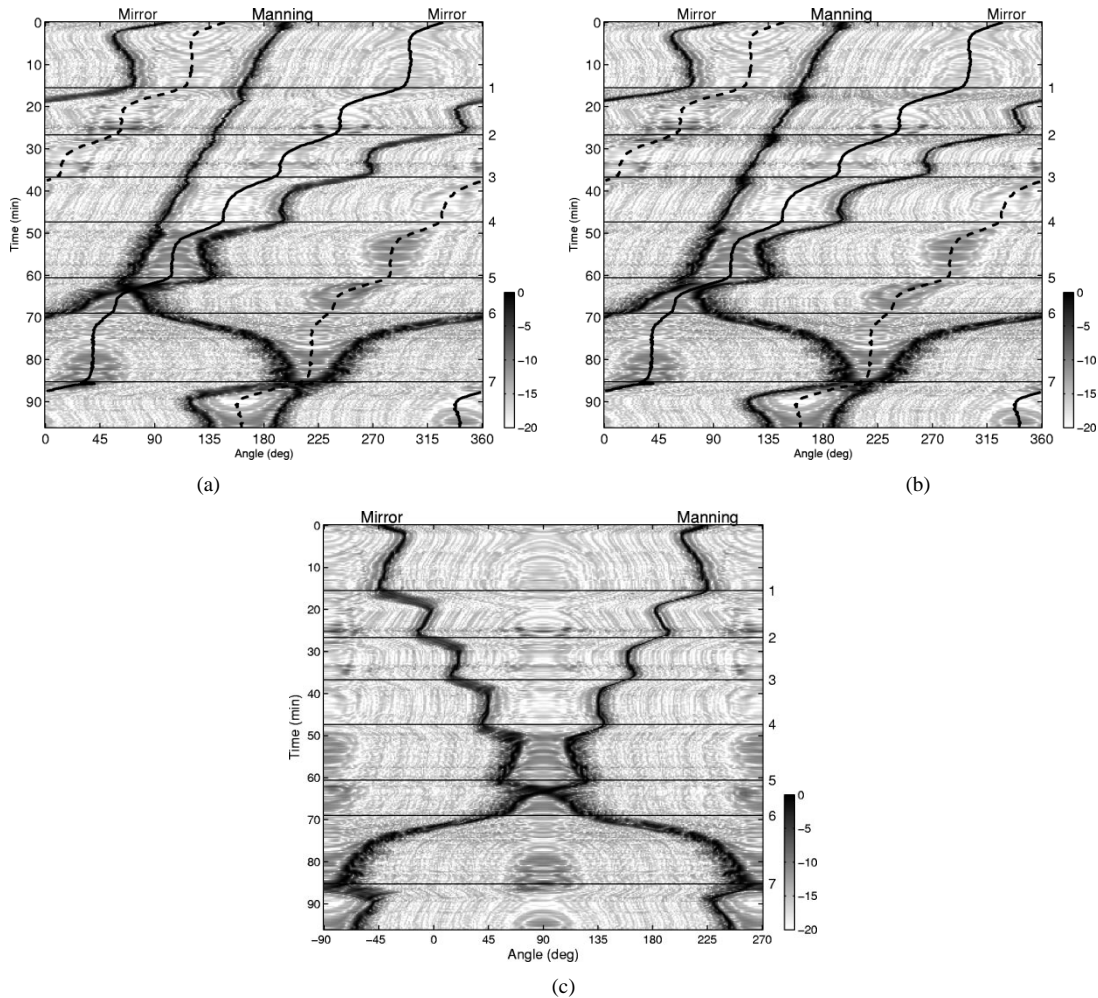


Fig. 6. Conventional beamforming at 375 Hz (20-dB dynamic range) (a), (c) with and (b) without shape correction using true bearing [(a) and (b)] or local bearing (c). The angle to MANNING is as shown in Fig. 3(a) [for (a) and (b)] and Fig. 3(b) [for (c)]. The horizontal lines indicate the start of a turn. The forward (solid black) and aft (dashed black) heading are also indicated.

- 3) The curvature of the array will often be less than the curvature of the ship course, as the array is smearing out the corners. This is empirically approximated by averaging the bow over 10 neighboring points, corresponding to a length of 1.5 times the array length.

The estimated bow just based on point 2) above is shown as the dotted curve in Fig. 5. After time delaying 1) and smoothing 3) the bow, a very close match (solid) to the acoustically estimated (dashed) bow is observed. The acoustically estimated bow is based on the shape of the wavefront of the loud broad-band acoustic pulse (see the Appendix). This is very accurate, but such a source is likely only available under ideal experimental configurations. From Fig. 5 it is seen that, after about a 3-min startup, a very good fit is obtained for the first 60 min where the array is not in the near-field of the source. Thus, it is feasible to estimate bow based on GPS.

## V. BEAMFORMING

Having outlined the array shape model and verified it with broad-band acoustic data, it is now experimentally demonstrated that both the conventional and the WNC adaptive beamformer can benefit from an accurate shape estimation.

For the curved array, the steering vectors  $\mathbf{d}$  are computed based on the phase delay for each of the  $N = 128$  hydrophones

$$\exp\left(i \frac{\omega}{c} y_{\gamma}\right) \quad (5)$$

where  $c$  is the reference sound speed and  $y_{\gamma}$  is the component perpendicular to the wavefront as determined by (4). The range to the source is not modeled.

### A. Conventional Beamformer

1) *Approach*: For the observed data on the 128-element HLA, the fast Fourier transform (FFT) length was chosen sufficiently long so that both the pulse and multipaths are included. Thus, a 16 K-point FFT length (corresponding to 2.6 s,  $\Delta f = 6000/2^{14} = 0.36$  Hz) was selected. There has been no attempt made to optimize the processing parameters. The conventional beamformer power then is computed as

$$\Phi_{\text{CBF}} = \mathbf{w}^{\dagger} \mathbf{C} \mathbf{w} \quad (6)$$

where  $\mathbf{w} = \mathbf{W} \mathbf{d} / N$  and  $\mathbf{d}$  is the complex steering vector as determined by (5).  $\mathbf{W}$  is a diagonal matrix of normalized shading weights; a Kaiser–Bessel window with  $\alpha = 1.5$  was used (a Hanning window gave similar performance).  $\mathbf{C}$  is the data covariance matrix. Due to the transient nature of the signal, a single-snapshot covariance matrix is used.

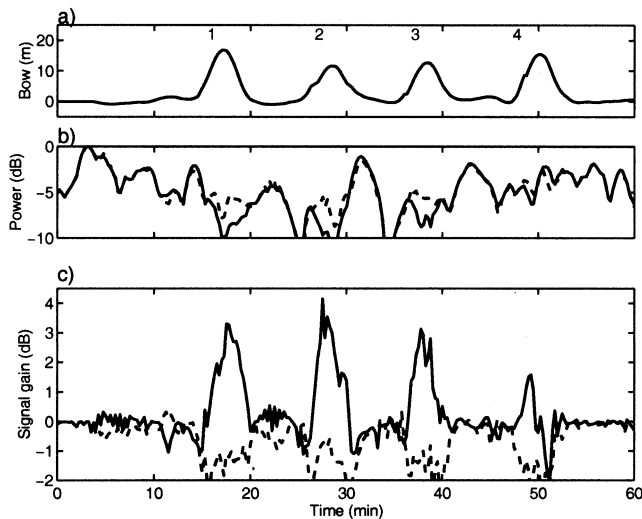


Fig. 7. Array power versus time. (a) Array bow estimated from GPS (from Fig. 5). (b) Beamformer output power without (solid) or with (dashed) shape correction (decibels relative to maximum). (c) Signal gain over the straight array with shape correction. Only the first 60 min is shown as the horizontal array then approaches the near-field of the source.

2) *Results:* After showing the processing of the data below, it will be demonstrated that beamforming with shape correction here resulted in: 1) 5-dB signal gain; 2) 4-dB difference between true and mirror source; and 3) smaller 3-dB bandwidth.

The conventional beamformer power (decibels) as a function of time and bearing with shape correction is shown in Fig. 6. The plot is normalized so that the maximum across angle at each ping is 0 dB. Fig. 6(a) and (b) displays true bearing, where true bearing is the angle to the source relative to North. The start of each turn is indicated by horizontal lines. Roughly, the array is curved up to 5 min after the turn and is straight for the rest of the leg. Forward heading of the array (solid black), determined as the average of head and tail compasses, and aft heading (forward heading  $+180^\circ$ ) (dashed black) are indicated. These two lines indicate endfire locations of the array, where the array is less able to locate a source. Also, for a straight array, the angle to the source will be mirrored around these lines.

For the first 50 min, the signal is within  $45^\circ$  to broadside and thus the planewave beamforming works well. For later times, the array goes through endfire (around  $t = 65$  min and  $t = 85$  min) and is in the near-field (around  $t = 72$  min). Both of these effects makes the processing at later times less robust. We are not modeling the range dependence which are important in the nearfield.

The conventional beamformer power in the direction of the Manning source as a function of time with (dashed line) or without (solid line) shape correction is shown in Fig. 7(b). Subtracting these powers gives up to a 4-dB signal gain when the array is turning [solid line, Fig. 7(c)]. Using the negative bow, corresponding to mirror source, a 2.5-dB signal loss is observed [dashed line, Fig. 7(c)]. Effectively, the array curvature removes the left/right ambiguity.

To verify this performance, a simple simulation with identical geometry and assuming the target at  $45^\circ$  to broadside on a bowed array is carried out (see Fig. 8). If the bow of the array

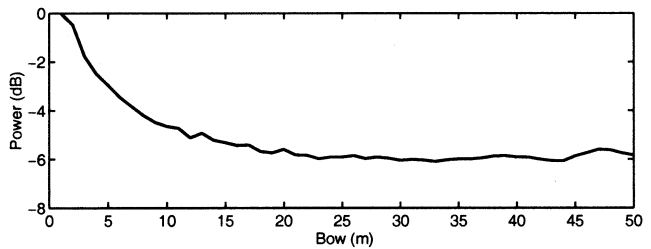


Fig. 8. Conventional beamforming power versus bow using simulated data.

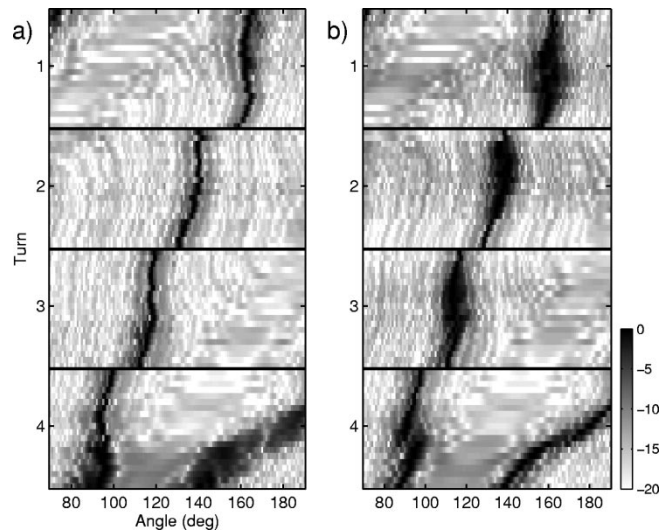


Fig. 9. Conventional beamforming using the first 5 min of each of the first four turns (a) with and (b) without shape correction. The plot is normalized so that the maximum across the angle at each ping is 0 dB.

is neglected in the processing, up to a 6-dB loss in power is suffered.

The importance of the shape estimation is emphasized by focusing on the 5 min after the start of each turn in Fig. 6; a time-angle contour plot around the source direction shows clearly how the beamwidth is narrower when shape correction is applied, Fig. 9. This is similar to the wider 3-dB beamwidth that can be observed for the mirror track [4]. The latter feature can be seen in Fig. 6(a) and (c) and could be used to identify left/right ambiguity.

The left/right symmetry which is usually present in the ambiguity surfaces is broken by three effects: 1) using a curved array; 2) using a true bearing; and 3) larger 3-dB beamwidth for the mirror as mentioned above. The first two effects are most important and will be examined.

- 1) During the turn, it is seen from Fig. 7(c) that the signal gain is 5 dB more for the true angle than for the mirror angle. For comparison, the result of beamforming using a straight array is shown in Fig. 6(b).
- 2) The true bearing display helps decide between the true track and the mirror image, as a ship traveling in a straight course will remain so in this display. To see this, compare the conventional beamformer power in Fig. 6(a) to the conventional beamformer power in Fig. 6(c) where the angle now is in a local coordinate system with  $-90^\circ$  being aft endfire and the angle increasing in the counter-clockwise direction. When the source is at endfire (around

$t = 65$  min and  $t = 85$  min), the angle to the source is smeared out.

### B. WNC Adaptive Beamformer

Adaptive beamforming provides higher resolution and better side lobe suppression than conventional beamforming. However, adaptive beamforming is more sensitive to mismatch and without shape correction no detection might be obtained. Further, snapshot deficient processing is severely biased. To explore these issues, beamforming is carried out with the WNC adaptive processor [19], [20].

1) *Approach*: The WNC beamformer is based on the minimum variance distortionless response (MVDR) beamformer. The weights for the MVDR processor are given by

$$\mathbf{w} = \frac{\mathbf{R}^{-1}\mathbf{d}}{\mathbf{d}^\dagger\mathbf{R}^{-1}\mathbf{d}}. \quad (7)$$

The weights  $\mathbf{w}$  satisfy the constraint

$$\mathbf{w}^\dagger\mathbf{d} = 1. \quad (8)$$

$\mathbf{R}$  is the CSDM and usually is estimated by averaging over snapshots at a given frequency. Often  $\mathbf{R}$  is singular due to few available snapshots and then the inverse cannot be computed. This problem can be remedied by adding diagonal loading to  $\mathbf{R}$ . In the WNC processor, the amount of diagonal loading varies for each look angle

$$\mathbf{w} = \frac{(\mathbf{R} + \epsilon\mathbf{I})^{-1}\mathbf{d}}{\mathbf{d}^\dagger(\mathbf{R} + \epsilon\mathbf{I})^{-1}\mathbf{d}} \quad (9)$$

where  $\epsilon$  is chosen such that the white noise gain  $G$  is larger than the constraint value  $\delta^2$

$$\mathbf{G} = \frac{1}{\mathbf{w}^\dagger\mathbf{w}} > \delta^2. \quad (10)$$

A typical value for  $\delta^2$  is 2 dB down from  $10 \log N$  where  $N$  is the number of sensors.

Here, the WNC adaptive beamformer is implemented in two steps. First, a CSDM  $\mathbf{R}$  is estimated for use in computing  $\mathbf{w}$  in (9). Since we have LFM transmission data available,  $\mathbf{R}$  is estimated as an ensemble average of data vector outer products over neighboring frequencies [21], [22]. Then, the WNC beamformer output power is computed as

$$\Phi_{\text{WNC}} = \mathbf{w}^\dagger\mathbf{C}\mathbf{w} \quad (11)$$

where  $\mathbf{C}$  is the data covariance matrix. It can be determined based on single narrow-band snapshot. This approach is mostly used here as many sources in the ocean are narrow-band. Alternatively,  $\mathbf{C}$  can be estimated based on averaging multiple frequencies, similar to  $\mathbf{R}$ .

Our approach differs from [21], [22] in that we only use frequency averaging for  $\mathbf{R}$ , but not for computing the output power. Frequency averaging of  $\mathbf{R}$  increases the number of nonzero eigenvalues of the covariance matrix and is a type of covariance matrix tapering for broadening nulls [26]. This will cause broadening of the signal.

As will be shown below, good results were obtained when the matrix  $\mathbf{R}$  was estimated using 21 frequency bins corresponding to a total bandwidth of 7.3 Hz. For much fewer frequency bins (3 or 5 frequencies), the results were not as stable, and for a larger frequency band (101 frequencies), the power appears more smeared out.

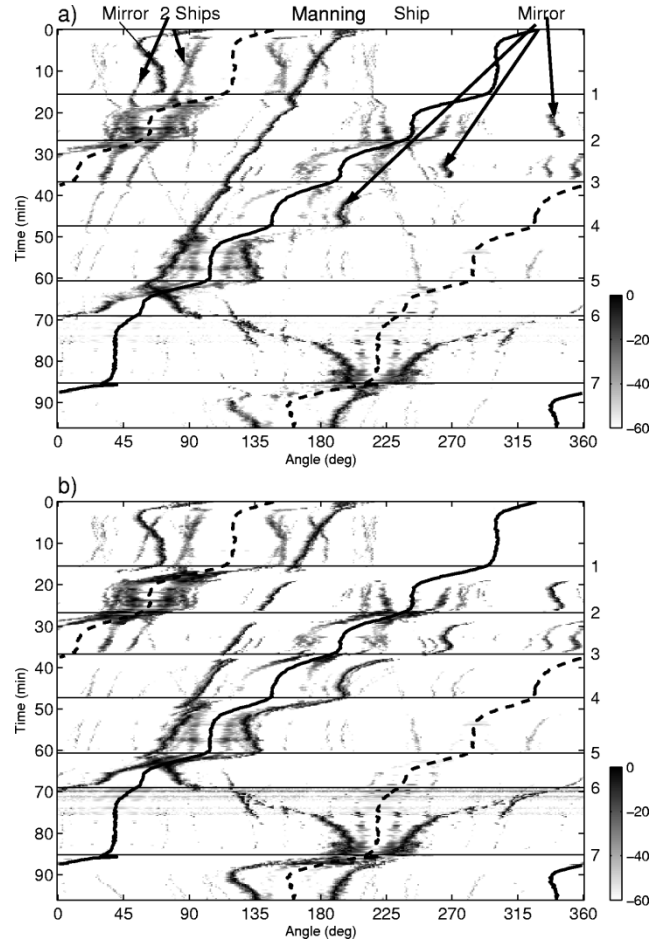


Fig. 10. WNC adaptive beamforming (375 Hz) in true bearing (a) with and (b) without shape correction.

The adaptive processing is severely biased due to snapshot-deficient processing [1], [2]. For small  $\epsilon$ , the bias depends quadratically on the diagonal loading, i.e.,  $20 \log_{10} \epsilon$  and for large  $\epsilon$  there is little bias [26]. For MVDR, the bias is the same in all directions, as  $\epsilon$  is constant. However, for the WNC, due to larger  $\epsilon$  in the source direction, this direction is only slightly biased. The variation in bias is the main reason for the large dynamic range observed in the following results.

2) *Results*: First the basic WNC adaptive beamforming processing is shown on the whole time series. Then, it is shown that only with shape correction can the source be tracked during a turn and the mirror source is not detected. The left/right ambiguity is then nonmanifest. The issues of beamwidth, broad-band incoherent processing and the ability to track several ships in the presence of a loud source are discussed.

The results from the WNC processing are shown with [Fig. 10(a)] and without [Fig. 10(b)] shape correction. The matrix inversion for the steering vectors is stabilized using the CSDM estimated from the data at 21 frequency bins in a 7.3-Hz band centered around 375 Hz. The angle to MANNING is as shown in Fig. 3(a). The mirror track of the source is very weak during turns for the curved array while the true track is quite well defined also during the turns. Without shape correction [Fig. 10(b)], the dynamic range is reduced strongly when the array is turning. This shows up as gray horizontal

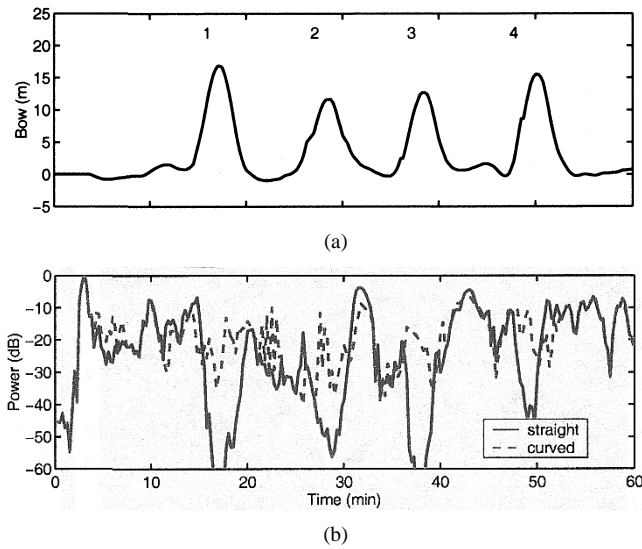


Fig. 11. Array power versus time. (a) Array bow estimated from GPS. (b) Beamformer output power assuming a straight array (solid) or curved array (dashed) (decibels relative to maximum).

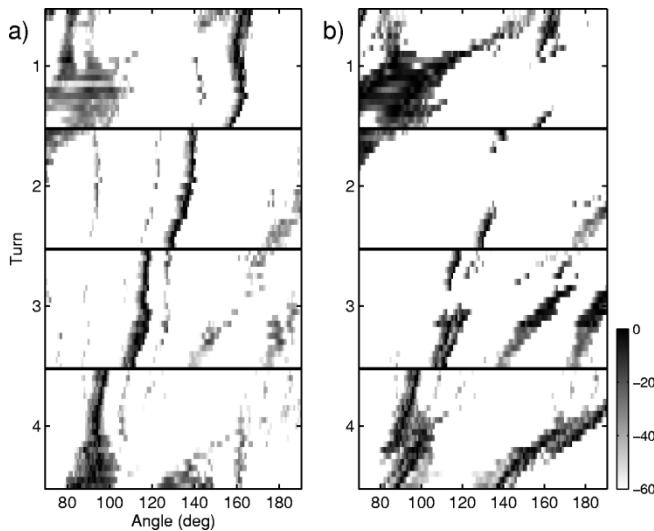


Fig. 12. WNC adaptive beamforming with focus on the first four turns (a) with and (b) without shape correction.

lines in the contour plots. In the near-field, the curvature of the wavefront is so large that it is not possible to get good results when processing assuming plane waves. The dynamic range with WNC processing is much larger than that for conventional beamforming (60 dB instead of 20 dB) and thus weaker sources now also can be seen. The weaker sources are much better observed when the data are processed with shape correction.

Similar to Fig. 7 for conventional beamforming, the WNC output power in the direction of the Manning source is plotted with and without shape correction (Fig. 11). Without shape correction (solid line), the beamformer output power drops significantly when the array is turning. However, with shape correction (dashed line), the power remains high [Fig. 11(b)].

Focusing on the 5 min after the start of each turn, a time-angle contour plot of the WNC output power shows clearly how the signal is followed very well when shape correction is used

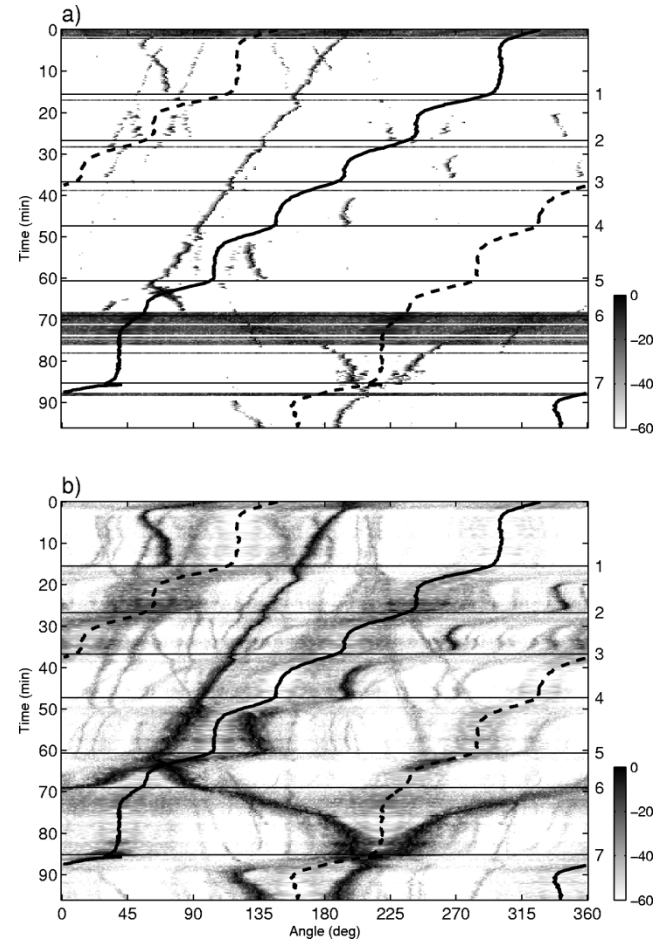


Fig. 13. WNC processing (375 Hz) in true bearing with shape correction. The matrix inversion for the steering vector is stabilized using the covariance matrix estimated from the data using (a) five bins [1.4-Hz band] and (b) 101 bins [36-Hz band] centered around 375 Hz.

[Fig. 12(a)]. Without shape correction [Fig. 12(b)], the signal is sometimes lost. Due to the normalization, this shows up as a white area (noise floor) in the middle of turn 1-3.

Using a narrower frequency band for the steering vector [Fig. 13(a) using five frequency bins, 1.4-Hz bandwidth] did not give as stable results. Several of the time frames gave noisy output power across all angles [horizontal dark lines in Fig. 13(a)] with no clear estimate of the angle to the source. By decreasing the dynamic range to 10 dB instead of 60 dB, it is possible to track the source but not other ships. Using a much larger frequency band [Fig. 13(b) using 101 frequency bins, 36-Hz bandwidth] does stabilize the matrix inversion but now the results are more smeared out as the frequency interval is wide.

When computing the WNC output power, it also is possible to use the frequency-averaged CSDM  $\mathbf{R}$  in (11). This is identical to an incoherent averaging of the narrow-band output powers for a common broadband weight vector  $\mathbf{w}$ . The result of this broadband WNC (see Fig. 14) is here slightly better than the narrow-band output, since a few more weak ship tracks can be seen than are visible in Fig. 10. The true track can easily be seen, since for all the ships the mirror track is lost during the turn and due to the true bearing display [point 2) in Section V-A2].

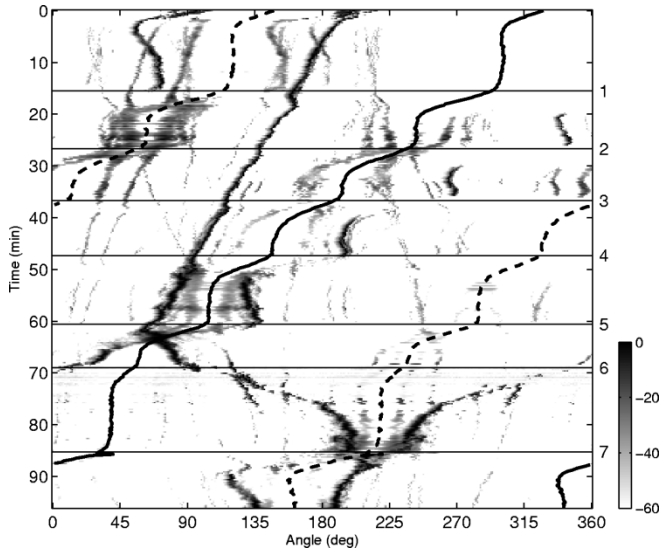


Fig. 14. WNC processing in true bearing with shape correction. The same CSDM  $\mathbf{R}$  (based on 21 frequency bins in a 7.3-Hz band) is used for the computing beamformer output power as well as the weight vectors.

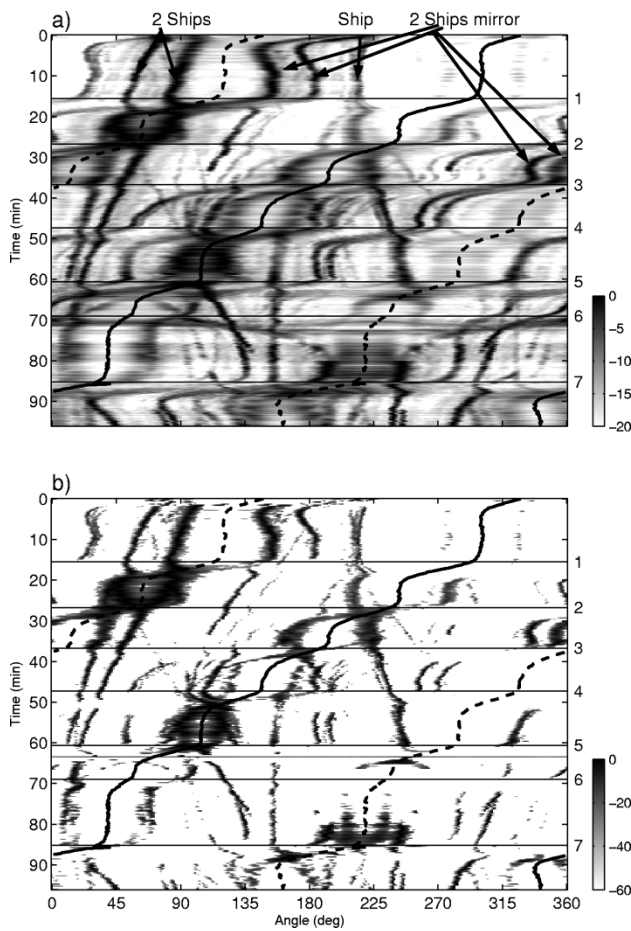


Fig. 15. (a) Conventional beamforming (20-dB dynamic range) and (b) WNC processing (60-dB dynamic range) in true bearing and by incoherent summing of the power at 130, 140, and 150 Hz.

For processing below the 150–500 Hz LFM sequence, narrow-band CSDMs were estimated based on a 2K-point FFT length (corresponding to 0.3 s,  $\Delta f = 6000/2^{11} = 3$  Hz). For

a 4-s data length, this provides 12 snapshots. The result of incoherent processing the data at 130, 140, and 150 Hz is shown in Fig. 15. Note that many of the sources at 375 Hz also can be seen at these lower frequencies. Two ships appear to transition from  $90^\circ$  ( $t = 0$  min) toward  $0^\circ$  ( $t = 70$  min). A track from  $200^\circ$  ( $t = 0$  min) toward  $250^\circ$  ( $t = 60$  min) can also be seen.

Real-time WNC beamforming is realistic. Inversion of  $(\mathbf{R} + \epsilon\mathbf{I})^{-1}$  is done using SVD, and this is only needed once for all look directions. Iterations are only necessary in the directions of interferers or sources. Evaluating the WNC for 360 look directions took 1.2 s for a MATLAB code on a 1.8-GHz Pentium IV. The MVDR was just 2% faster.

## VI. CONCLUSION

Based on real data, it is demonstrated that adaptive beamforming is feasible on a turning array.

A towed array can be modeled as a linear rotation of the array from the ship's course and a parabolic bow. The linear rotation can be determined from compasses in the array. The bow of the array can be modeled based on time delaying and smoothing of the coordinates from the ship's GPS.

The use of a curved array model is superior when the ship is turning and the array is nonstraight. Plotting the beamforming results in a time-true bearing (true bearing is the bearing relative to North) coordinate system makes it very easy to resolve the left–right ambiguity. During most turns, the left–right ambiguity is resolved using the parabolic model of array shape.

A common problem when using adaptive beamforming is that the steering vector depends on a matrix inversion of the CSDM which might be singular. For the WNC processor, it was shown that the steering vector computation can be stabilized using a frequency-averaged CSDM.

The proposed algorithms have been tested on real data with the tow-vessel making  $45^\circ$  turns with a 500-m curvature radius. While turning, the improvement in performance over the assumption of a straight array geometry was up to 5 dB for the conventional beamformer and considerably larger for the WNC adaptive beamformer.

## APPENDIX

### MATHEMATICAL MODEL OF THE ARRAY SHAPE

The tow ship and array geometry are shown in Fig. 4. The main coordinate system has the  $x_v$  axis pointing in the aft direction from the vessel.

The turning array is modeled as a rotation  $\beta$  around the first hydrophone from the ship's aft heading to the axis defined by the first and last hydrophone and a parabolic bow  $a$  [see Fig. 4(a)]. In a local coordinate system with the  $x_a$  axis passing through first and last hydrophone of the array [Fig. 4(a)], the offsets ( $y$  coordinate) of each array element are given by

$$y_a = \frac{4a}{L_a^2} (L_a - x_a)x_a \quad (\text{A1})$$

where  $L_a$  is the projection of the array along the  $x_a$  axis. The maximum curvature of this array is

$$\kappa = \frac{\partial^2 y_a}{\partial x_a^2} = -\frac{8a}{L_a^2}. \quad (\text{A2})$$

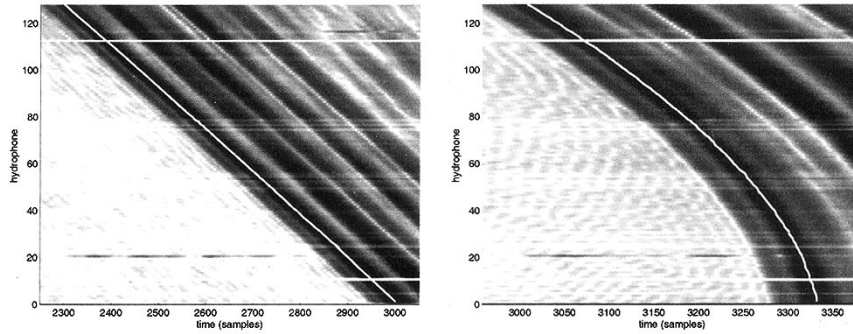


Fig. 16. Matched filtered time series (dB) for a straight array just before Turn 1 (top,  $t = 15$  min, ping 60); curved array (middle,  $t = 17.5$  min, ping 70); straight array in the nearfield (bottom,  $t = 70.5$  min, ping 274). The curvature of the array is based on tracing the maximum of the matched filter (white). Hydrophone 1 is closest to the ship.

The arc length of the array  $L_s$  (this is also the length of the straight array) in [25, eq. 38] is related to the length of the array measured along the  $x_a$  axis  $L_a$  as

$$\begin{aligned} L_s &= \int_{x=0}^{L_a} \sqrt{1 + \left(\frac{\partial y}{\partial x}\right)^2} dx \\ &= \frac{L_a}{2} \left[ \sqrt{1 + b^2} + \frac{1}{2b} \ln \frac{\sqrt{1 + b^2} + b}{\sqrt{1 + b^2} - b} \right] \\ &\approx L_a + \frac{8}{3} \frac{a^2}{L_a} \end{aligned} \quad (\text{A3})$$

where  $b = 4a/L_a$ . The  $x$  coordinate of each element for a bowed array  $x_a$  can then be related to the element position along a straight array  $x_s$

$$x_a = x_s \frac{L_a}{L_s}. \quad (\text{A4})$$

A plane wave impinging at an angle  $\gamma$  between the wavefront and the array ( $x_a$  axis) will see an equivalent array where the  $x_\gamma$  axis is parallel to the wavefront and the  $y_\gamma$  axis perpendicular [Fig. 4(b)]

$$x_\gamma = x_a \cos \gamma - y_a \sin \gamma \quad (\text{A5})$$

$$y_\gamma = x_a \sin \gamma + y_a \cos \gamma. \quad (\text{A6})$$

Only the direction perpendicular to the wavefront  $y_\gamma$  gives a phase difference across the array

$$y_\gamma = \frac{4a \cos \gamma}{L_a^2} (L_a - x_a)x_a + x_a \sin \gamma \quad (\text{A7})$$

$$= -\frac{4a \cos \gamma}{L_a^2} \left( \frac{L_a x_s}{L_s} \right)^2 + \frac{L_a x_s}{L_s} \left[ \frac{4a \cos \gamma}{L_a} + \sin \gamma \right]. \quad (\text{A8})$$

Using  $x_s = nd$ , where  $n = \{0, \dots, 127\}$  and  $d$  is the element spacing,  $y_\gamma$  can be further developed as

$$y_\gamma = -\frac{4a \cos \gamma}{L_s^2} (dn)^2 + dn \left[ \frac{4a \cos \gamma}{L_s} + \frac{L_a}{L_s} \sin \gamma \right]. \quad (\text{A9})$$

Assuming a plane wave arrival structure on the array, the angle and array curvature can be estimated from the acoustic measured bow. Based on the maxima of the matched filtered time series received on the array, a parabola is fit

$$y = An^2 + Bn + C \quad (\text{A10})$$

where  $y$  is derived from travel time ( $ct$ ) and  $n$  is hydrophone number.

From the estimated parabola we obtain

$$A = -\frac{4a \cos \gamma}{L_s^2} d^2 \quad (\text{A11})$$

$$\begin{aligned} B &= d \left( \frac{4a \cos \gamma}{L_s} + \frac{L_a}{L_s} \sin \gamma \right) \\ &= d \left( -\frac{AL_s}{d^2} + \frac{L_a}{L_s} \sin \gamma \right). \end{aligned} \quad (\text{A12})$$

The array bow  $a$  and angle  $\gamma$  (or the maximum curvature) can then iteratively be determined as

$$a = -\frac{AL_s^2}{4d^2 \cos \gamma} \quad (\text{A13})$$

$$\gamma = \text{Arcsin} \left( \frac{L_s}{L_a} \left( \frac{AL_s}{d^2} + \frac{B}{d} \right) \right) \quad (\text{A14})$$

$$\approx \text{Arcsin} \left( \left( 1 + \frac{8}{3} \frac{a^2}{L_s} \right) \left( \frac{AL_s}{d^2} + \frac{B}{d} \right) \right). \quad (\text{A15})$$

Note that, for endfire  $\cos \gamma = 0$  and a nonzero acoustic bow  $A$ , the bow of the array  $a$  will approach infinity. By use of acoustics, it is not possible to determine  $\beta$ .  $\beta$  can, however, often be estimated as the difference between the ship's course and the compass heading in the arrays.

To show that it is feasible to estimate the bow using the acoustic wavefronts, this information will be extracted from the received LFM sequence on the array.

First, the received signal was matched filtered with a 150–500-Hz LFM sequence (Fig. 16). The shape of the array is then determined based on tracking of the maximum matched filtered output (white line) subject to a maximum time delay between the neighboring phones corresponding to the separation distance (2 m). The shape of the array as seen from the incoming wave for three pings is shown in Fig. 16. Note that apart from the sign of the curvature, it is impossible to see any difference between a curved array in the farfield [Fig. 16(b)] and a straight array in the near-field [Fig. 16(c)] where the wavefront is curved. Thus, when estimating the array curvature, the array should be in the farfield or the range to the source should be known.

Based on the curve for each ping, a least squares fit to a parabola [See (A10)] was obtained and then the angle  $\gamma$  [See (A15)] and bow  $a$  [See (A13)] can be obtained. Since the transmission time of the source was known, the travel time [represented by  $C$  in (A10)] and range to the source also were esti-

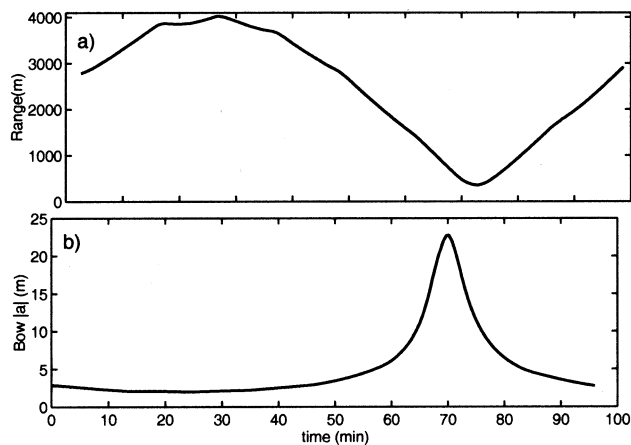


Fig. 17. (a) Range and (b) estimated magnitude of equivalent bow due to the source being in the near-field of the HLA based on GPS.

mated. However, for estimating just  $A$  and  $B$  the reference time can be chosen arbitrarily.

Following this procedure, the bow of the array is estimated as shown by the dashed line in Fig. 5 (the lines determined by GPS are discussed later). The first four turns are very well determined. Around turn 6 (70–80 min), the array is in the near field and the bow is incorrectly determined. For turns 5 and 7 the array passes through endfire. At endfire (and nonzero acoustic bow), the bow of the array will become infinite if estimated acoustically.

Assuming the source is at range  $r$  from the array, the equivalent acoustic bow  $|a_{\text{nf}}|$  due to the source being in the near-field can be estimated as

$$|a_{\text{nf}}| = \frac{L_s^2}{8r} \quad (\text{A16})$$

which is obtained by requiring the same curvature of the array as the wavefront at broadside. This relation is shown in Fig. 17. Note that we cannot estimate the sign of the curvature since a wavefront approaching from the left or right is received identically on the array. Note also that, if the array shape is known, the measured curvature of wavefront on the array can be used to determine the range to the source.

#### ACKNOWLEDGMENT

The experimental data for this work were provided by SACLANTCEN.

#### REFERENCES

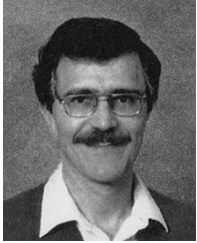
- [1] A. B. Baggeroer and H. Cox, "Passive sonar limits upon nulling multiple moving ships with large aperture arrays," in *Proc. 33rd IEEE Asilomar Conf. Signal, Systems, and Computers*, vol. 1, 1999, pp. 103–108.
- [2] H. Cox, "Multi-rate adaptive beamforming (MRABF)," in *Proc. IEEE Sensor Array and Multichannel Signal Processing Workshop*, 2000, pp. 306–309.
- [3] W. S. Hodgkiss, "The effects of array shape perturbation on beamforming and passive ranging," *IEEE J. Oceanic Eng.*, vol. OE-8, pp. 120–130, 1983.
- [4] D. M. Caveny, D. R. Del Balzo, J. H. Leclere, and G. E. Loup, "Performance of sinusoidally deformed hydrophone line arrays," *J. Acoust. Soc. Amer.*, vol. 104, pp. 2203–2209, 1998.
- [5] H. Bucker, "Beamforming a towed line array of unknown shape," *J. Acoust. Soc. Amer.*, vol. 63, pp. 1451–1454, 1978.

- [6] B. G. Ferguson, "Sharpness applied to the adaptive beamforming of acoustic data from a towed array of unknown shape," *J. Acoust. Soc. Amer.*, vol. 88, pp. 2695–2701, 1990.
- [7] —, "Remedying the effects of array shape distortion on the spatial filtering of acoustic data from a line array of hydrophones," *IEEE J. Oceanic Eng.*, vol. 18, pp. 565–571, 1993.
- [8] D. E. Wahl, "Towed array array shape estimation using frequency-wavenumber interpolation," *IEEE J. Oceanic Eng.*, vol. 18, pp. 582–590, 1993.
- [9] S. E. Dosso and B. J. Sotirin, "Optimal array element localization," *J. Acoust. Soc. Amer.*, vol. 106, pp. 3445–3459, 1999.
- [10] N. Ma and J. T. Goh, "Eigen structure based array shape estimation using sources in unknown locations," in *Proc. IEEE Oceans*, 2000, pp. 1895–1900.
- [11] S. E. Dosso and M. Riedel, "Array element localization for towed marine seismic arrays," *J. Acoust. Soc. Amer.*, vol. 110, pp. 955–966, 2001.
- [12] D. A. Gray, B. D. O. Anderson, and R. R. Bitmead, "Towed array shape estimation using Kalman filters—Theoretical models," *IEEE J. Oceanic Eng.*, vol. 18, pp. 543–556, 1993.
- [13] H.-Y. Park, W. T. Oh, D.-H. Youn, and C. Lee, "Performance improvement of array shape estimation using spline interpolation," in *Proc. IEEE Oceans*, 2001, pp. 1715–1718.
- [14] N. L. Owsley, "Shape estimation for a flexible underwater cable," in *Proc. IEEE EASCON*, 1981, pp. 20–23.
- [15] P. Felisberto and S. M. Jesus, "Towed array beamforming during ship's maneuvering," *Proc. IEE Radar, Sonar Navig.*, vol. 143, pp. 210–215, 1996.
- [16] J. P. Ianniello and J. M. Tattersall, "Broadband shallow water localization using a mobile array," in *Experimental Acoustic Inversion Methods for Exploration in the Shallow Water Environment*, A. Caiti, S. Jesus, J. P. Hermand, and M. B. Porter, Eds. Amsterdam, The Netherlands: Kluwer, 2000.
- [17] R. M. Kennedy, "Crosstalk dynamics of a long cable towed in the ocean," in *Proc. IEEE Oceans*, 1981, pp. 966–970.
- [18] A. P. Dowling, "The dynamics of towed flexible cylinders: Part 2. Negative buoyant elements," *J. Fluid. Mech.*, pp. 533–571, 1988.
- [19] H. Cox, R. M. Zeskind, and M. M. Owen, "Robust adaptive beamforming," *IEEE Trans. Acoust., Speech, Signal Processing*, vol. ASSP-35, pp. 1365–1576, 1987.
- [20] R. A. Graham, "ABF algorithms implemented at ARL: UT," Applied Research Laboratory, Univ. Texas at Austin, ARL-TR-92-7, 1992.
- [21] J. Krolik and D. Swingler, "Multiple broad-band source location using steered covariance matrices," *IEEE Trans. Acoust., Speech, Signal Processing*, vol. 37, pp. 1481–1494, Oct. 1989.
- [22] D. E. Grant, J. H. Gross, and M. Z. Lawrence, "Cross-spectral matrix estimation effects on adaptive beamforming," *J. Acoust. Soc. Amer.*, vol. 98, pp. 517–524, 1995.
- [23] P. Gerstoft and D. F. Gingras, "Parameter estimation using multi-frequency range-dependent acoustic data in shallow water," *J. Acoust. Soc. Amer.*, vol. 99, pp. 2839–2850, 1996.
- [24] H. Bucker and P. A. Baxley, "Automatic matched-field tracking with table lookup," *J. Acoust. Soc. Amer.*, vol. 106, pp. 3226–3230, 1999.
- [25] P. Gerstoft. (1997) SAGA users guide 2.0, an inversion software package. SACLANT Undersea Research Centre, SM-333
- [26] H. C. Song, W. A. Kuperman, W. S. Hodgkiss, P. Gerstoft, and J. Kim, "Null broadening with snapshot-deficient covariance matrices," *IEEE J. Oceanic Eng.*, submitted for publication.



**Peter Gerstoft** received the M.Sc. and Ph.D. degrees from the Technical University of Denmark, Lyngby, in 1983 and 1986, respectively, and the M.Sc. degree from the University of Western Ontario, London, ON, Canada, in 1984.

From 1987 to 1992, he was employed at Ødegaard and Danneskiold-Samsøe, Copenhagen, Denmark, working on forward modeling and inversion for seismic exploration, with a year as a Visiting Scientist at the Massachusetts Institute of Technology, Cambridge. From 1992 to 1997, he was Senior Scientist at SACLANT Undersea Research Centre, La Spezia, Italy, where he developed the SAGA inversion code, which is used for ocean acoustic and electromagnetic signals. Since 1997, he has been with Marine Physical Laboratory, University of California, San Diego. His research interests include global optimization and modeling and inversion of acoustic, elastic, and electromagnetic signals.



**William S. Hodgkiss** (S'68–M'75) was born in Bellefonte, PA, on August 20, 1950. He received the B.S.E.E. degree from Bucknell University, Lewisburg, PA, in 1972 and the M.S. and Ph.D. degrees in electrical engineering from Duke University, Durham, NC, in 1973 and 1975, respectively.

From 1975 to 1977, he worked with the Naval Ocean Systems Center, San Diego, CA. From 1977 to 1978, he was a faculty member in the Electrical Engineering Department, Bucknell University. Since 1978, he has been a Member of the Faculty of the Scripps Institution of Oceanography, University of California, San Diego, and on the staff of the Marine Physical Laboratory where currently he is Deputy Director. His present research interests are in the areas of adaptive array processing, propagation modeling, and environmental inversions with applications of these to underwater acoustics and electromagnetic wave propagation.

Dr. Hodgkiss is a Fellow of the Acoustical Society of America.



**W. A. Kuperman** has done theoretical and experimental research in ocean acoustics and signal processing at the Naval Research Laboratory, SAACLANT Undersea Research Centre, La Spezia, Italy, and the Scripps Institution of Oceanography (SIO), University of California, San Diego. Presently he is a Professor at SIO and Director of its Marine Physical Laboratory.



**Heechun Song** (M'02) received the B.S. and M.S. degrees in marine engineering and naval architecture from Seoul National University, Korea, in 1978 and 1980, respectively, and the Ph.D. degree in ocean engineering from the Massachusetts Institute of Technology, Cambridge, in 1990.

From 1991 to 1995, he was with Korea Ocean Research and Development Institute. Since 1996, he has been a member of the scientists of the Marine Physical Laboratory/Scripps Institution of Oceanography, University of California, San Diego. His research interests include time-reversed acoustics, robust matched field processing, and wave propagation physics.



**Martin Siderius** received the B.S. degree in physics from Western Washington University, Bellingham, WA, in 1986 and the M.S.E.E. and Ph.D. degrees in electrical engineering from the University of Washington, Seattle, in 1992 and 1996, respectively.

He worked as an Engineer for Baird Corporation, Bedford, MA, from 1986 to 1987 and for Bio-Rad, Cambridge, MA, from 1987 to 1990. From 1990 to 1996, he was a Research Assistant with the Applied Physics Laboratory, University of Washington. From 1996 to 2001, he was on the scientific staff in the Acoustics Department at the NATO SAACLANT Undersea Research Centre, La Spezia, Italy. He joined Science Applications International Corporation (SAIC), San Diego, CA, in July 2001 and is currently a Senior Scientist in the Ocean Sciences Division. His research interests include underwater acoustics and signal processing.



**Peter Lourcing Nielsen** received the M.S. degree in mechanical engineering from Aalborg University, Denmark, in 1989 and the Ph.D. degree from the Technical University of Denmark in 1993.

From 1993 to 1996, he was employed at the Technical University of Denmark on a European Union-funded MAST-II project concerning development and validation of numerical models for sound propagation in the ocean. He joined SAACLANT Undersea Research Centre, La Spezia, Italy, in 1996, working on numerical modeling and experimental data analysis of broad-band acoustic signals in shallow water. His interests are in numerical modeling of sound propagation in the ocean and geoacoustic inversion techniques of experimental acoustic data.